Dense nuclear matter with phenomenological short distance repulsion

Jesper Leong, Theo F. Motta,* and Anthony W. Thomas
CSSM and ARC Centre of Excellence for Dark Matter Particle Physics, Department of Physics, University of Adelaide, South Australia 5005, Australia

P. A. M. Guichon
Irfu, CEA, Université Paris-Saclay, F91191 Gif sur Yvette, France

(Received 21 December 2022; revised 16 March 2023; accepted 29 June 2023; published 24 July 2023)

The possibility of new short distance physics applicable inside the cores of neutron stars is incorporated into the equation of state generated by the quark-meson coupling model. The contribution of this new physics to the energy density is taken to be proportional to the amount of overlap between the quark cores of the baryons involved. With no change to the properties of symmetric nuclear matter at saturation density, including an incompressibility compatible with data on giant monopole resonances, one can sustain neutron stars with a maximum mass $M_{\rm max} > 2.1 M_\odot$, even when hyperons are included.

DOI: 10.1103/PhysRevC.108.015804

I. INTRODUCTION

Understanding the equation of state (EoS) of dense nuclear matter, namely the pressure as a function of energy density [1–3], $p = p(\epsilon)$, is one of the key challenges being addressed in modern nuclear theory. The EoS is well known in the low density region [4,5] and is believed to be constrained by perturbative QCD in the high density region [6–9]. In the intermediate region, the description of nuclear matter is still a matter of considerable debate. Heavy ion reactions have provided important constraints [10,11] up to densities of order several times the saturation density of symmetric nuclear matter, n_0. However, the matter formed in these collisions exists only for a short time and in a small volume, which introduces a degree of model dependence in the interpretation. Intense interest has shifted to long lived, cold neutron stars (NSs) because their core densities are expected to be as large as 4–10 times n_0. At such large densities we cannot be sure whether the matter is hadronic, quark matter, or some hybrid form [6,12,13]. Furthermore, as the matter in a NS is stable long term, to the extent that it is hadronic, one must satisfy the conditions of β equilibrium and hyperons must be present.

Of the more than 40 NS mass measurements, most center around the canonical mass of 1.4–1.5 $M_\odot$ [13–16]. These rely on the detection of a NS in a binary system [15,17,18]. Given the compactness and the extraordinary distances of these stars from Earth, mass and radius measurements on the same star still carry considerable uncertainty, making them suboptimal for constraining the EoS. Much of the focus has shifted to the heaviest of these stars, of which three are known; PSR J0348+0432 has a mass of $M = 2.01^{+0.04}_{-0.04} M_\odot$ [19], PSR J1614−2230 has a mass of $M = 1.908^{+0.016}_{-0.016} M_\odot$ [20], and PSR J0740+6620 has a mass of $M = 2.072^{+0.067}_{-0.066} M_\odot$ [21,22].

Measurements of NS radii are particularly difficult to narrow down [23]. However, the gravitational wave (GW) detection of GW170817 has placed new emphasis on the radii of NSs [24]. The NS merger event also allowed a totally new property, the tidal deformability, to be extracted from the waveform of the passing gravitational wave. For a 1.1–1.5 $M_\odot$ NS, the radius is largely independent of the mass. GW170817 involved component masses of $m_1 \in [1.18, 1.36] M_\odot$ and $m_2 \in [1.36, 1.58] M_\odot$, with radii for either star $R = 11.9 \pm 1.4$ km, making it highly likely that the event involved a binary NS system [24] (GW190425 may contain NSs but there is a high probability that the merger event has at least one black hole component [25]). The tidal deformability measured for GW170817, which was reported to be $\Lambda_{1.4} = 190^{+390}_{-120}$, is a measure of the quadrupole deformation of a spherical object caused by an inhomogenous external gravitational field [24]. GW measurements have the further advantage that they may offer insights concerning the presence of exotic matter in stars [26,27].

With the observation of NSs with masses $M \approx 2M_\odot$, many EoSs have been ruled out [19,21,28]. This is particularly true for those where hyperons are included. Under β equilibrium, hyperons are predicted to appear at or above $3n_0$, and, because they have low momentum near the threshold for their introduction, the pressure corresponding to a given energy density is lower than it would be without hyperons. Then the maximum mass of the star must be lower [13,17,18,29].

The quark-meson-coupling (QMC) model is unique amongst models for the binding of nuclear matter in that the change in the structure of any bound hadron, induced by the strong mean scalar field in medium [30,31], plays a key role. In particular, the resultant density dependent reduction in the coupling of baryons to the scalar field [32] is equivalent to introducing many-body forces [33]. The three-body force, in

*Now at the Institut für Theoretische Physik, Justus-Liebig-Universität Giessen.

particular, acts between all combinations of baryons, NNN, YNN, YYN, and YYY (with Y a hyperon), without the introduction of any new parameters. As a result of this three-body force, the QMC model predicted the existence of NSs with masses up to $2M_\odot$, with hyperons [34], three years before the first was observed [28].

Following the discovery of NSs with masses as large as $2M_\odot$, many possible solutions to what was regarded as the "hyperon puzzle" have been proposed. These include density dependent couplings, many body forces, and a possible phase transition from hadronic to deconfined quark matter [35,36]. By interpolating between accurate low ($n_B < 1.1n_0$) and high ($n_B > 40n_0$) density EoSs, several researchers have derived phenomenological EoSs matching heavy NS observations [6–9]. The requirement that the EoS approaches that of perturbative QCD at high densities has a distinct imprint on the speed of sound (c_s^2). Conformal matter has a limit of $c_s^2 < 1/3$ approaching from below, which suggests deconfined quark matter [6], although the appearance of hyperons has a similar signature [37,38].

The QMC model has been extensively developed since the prediction of high mass NSs with hyperons. The introduction of an isovector scalar meson did not dramatically change the predictions for NS properties, with the most significant change being an increase in the NS radius, for a given mass [39].

The energy density functional derived in the model [32,40] has been applied to the properties of even-even nuclei across the periodic table, with considerable success [41–44]. However, studies of the giant monopole resonances (GMRs) required the introduction of a term cubic in the scalar potential, which also lowered the incompressibility of nuclear matter [41]. The same term included in calculations of the EoS of dense nuclear matter tends to lower the maximum neutron star mass.

The parameters of the QMC model, associated with the exchanged mesons, are determined by the properties of infinite nuclear matter at saturation density [45]. On the other hand, the cores of the highest mass NSs involve much higher densities, where the finite-size baryons may overlap; something not included in the model. In that region nonperturbative gluon exchanges may lead to additional repulsion not accounted for by longer-range meson exchange. With this in mind, here we extend the QMC model to include a new, phenomenological, short-ranged repulsive force, which only affects the EoS at densities well above saturation density.

The structure of this paper is as follows. In Sec. II we summarize the calculation of the EoS of dense matter within the QMC model and introduce the new short distance repulsive force, designed to affect the EoS only at densities well above nuclear matter density. The results and concluding remarks are presented in Secs. III and IV.

II. THEORETICAL FRAMEWORK

In the MIT bag model, the quarks are confined in a spherical region, the interior of which is a strictly perturbative vacuum. In the QMC model the baryons retain their individual identity, even at higher densities [46,47]. One of the criticisms which Stone *et al.* [34] highlighted is the possibility that the QMC model would begin to breakdown at some unknown threshold density, where the hadrons start to overlap and eventually transition into quark matter. Actually, this may even be apparent at lower densities, of order $4n_0$, where nucleons geometrically touch [15]. Performing a lattice QCD calculation, Bissey *et al.* showed that three quarks in a baryon are connected by a Y-shaped flux tube [48]. Elsewhere a nonperturbative QCD vacuum exists, through which baryons are permitted to move freely. Thus a literal interpretation of the MIT bag model may not reflect the full physical picture of nuclear matter [34,40]. While this provides some justification for treating the baryons as nonoverlapping to higher densities than one might naively expect, one may anticipate that new interactions are likely to be needed eventually.

Berryman and Gardner proposed an extension to the standard model based upon gauging baryon number [49]. Their new short-ranged, repulsive quark-quark force was mediated by a vector boson coupling to baryon number B. Normally this would be suppressed by the highly repulsive short-range (0.4–0.6 fm) NN, YN, and YY potentials [50]. However, beyond saturation density, as the baryons start to *overlap*, the new interaction would have an affect on the resulting EoS [49,51]. To model this, a two-particle NN Yukawa potential was used, and Berryman and Gardner showed that the ensuing NS had a maximum mass of 2–2.2 $M_\odot$ [49].

In the QMC model the ω meson generates the short distance repulsion between baryons. However, as explained earlier, as the baryons begin to overlap we expect that there may be additional repulsion arising from nonperturbative QCD in the multiquark environment. Indeed, quark model studies over the past 40 years have shown that the Pauli exclusion principle, in combination with the increase in energy associated with hidden color configurations, leads to strong short distance repulsion between nucleons (see, e.g., Harvey [52]). This has been confirmed more recently by, for example, lattice QCD studies by the HAL Collaboration [53]. Low energy nucleon-nucleon scattering, which is used to constrain phenomenological descriptions of this in terms of, say, ω meson exchange, does not probe that short distance behavior [54] in detail and one might expect that this additional repulsion could be manifest in the much more dense systems at the core of a neutron star. To model these short distance interactions, we propose an additional, phenomenological term to be added to the QMC energy density, which only has appreciable effects at supranuclear densities. The functional form used to model the degree of overlap is taken to have a simple Gaussian form, given in Eq. (18), and is required to stiffen the EoS without changing the physics at saturation density.

Our summary of the key details of the QMC model follows closely the work of Motta *et al.* [39] and Guichon *et al.* [40]. The calculation is carried out in the Hartree-Fock approximation, with the inclusion of the isovector scalar meson, δ, as introduced by Motta *et al.* [39].

A. Energy density

In infinite nuclear matter, using the mean-field approximation, the effective mass of a baryon with flavor f is

given by

$$M_f^*(\bar{\sigma},\bar{\delta}) = \frac{\Omega_u N_u + \Omega_d N_d + \Omega_s N_s - z_0}{R_B} + BV_B + \Delta E_M. \quad (1)$$

R_B and V_B are the bag radius and volume respectively. Ω_i expresses the lowest eigenvalue for the three valence quarks, calculated in the local scalar mean fields (N_i denotes the number of u, d, or s quarks). The input parameters, determined at zero density, are B, α_s, and z_0. These are respectively the bag pressure, the strong coupling constant, which sets the size of the hyper-fine color interaction (ΔE_M), and the zero point gluon fluctuation terms. They are fitted to satisfy the mass of the free baryons and boundary conditions imposed by the MIT bag model [46,55]. Although the calculation of ΔE_M is complicated, it is essentially given by a spin matrix element multiplied by α_s divided by the bag eigenenergies of the pairs of quarks involved. It is the reduction in those eigenenergies in medium which leads to the enhancement of the hyperfine interaction there [56], which we include.

In the following, the baryon species with flavor f which we include are n, p, Λ, and $\Xi^{0,-}$, since previous calculations have shown that the $\Sigma^{0,\pm}$ and Δ baryons are absent for $n_B < 1.2$ fm^{-3} [34,57] (further explanations may be found in the results Sec. III B). The total number density is given by $n_B = \sum_f n_f$. Note that each flavor baryon f has a definite strangeness (S), isospin projection (m), and total isospin (t).

At the deepest level the QMC model takes into account the coupling of the lightest scalar (σ and δ) and vector (ω and ρ) mesons to the u and d quarks. Zweig's rule suggests that the coupling of these nonstrange mesons to the s quark should be suppressed, and in order to reduce the number of parameters in the model we set it to zero. We defer discussion of the phenomenological success of this approach, which provides some *a posteriori* justification, to Sec. III B. Of course, one does expect that there will be some mesons which couple to the strange quarks but $s\bar{s}$ mesons have masses in excess of 1 GeV and, in addition to the expected small coupling to nonstrange nucleons for such mesons, their large masses suggest that their effects will be strongly suppressed by short-range correlations. At the mean field level we solve self-consistently for the mass of the baryon using the MIT bag model but including the effect of the the σ and δ mesons. The resulting energy of a baryon with momentum $\vec{k}$ is then

$$E_f = \sqrt{M_f^*(\bar{\sigma},\bar{\delta})^2 + \vec{k}^2} + g_\omega^f \bar{\omega} + g_\rho^f I_m^f \bar{\rho}. \quad (2)$$

Here, the mean isoscalar and isovector scalar mean-fields are $\bar{\sigma}$ and $\bar{\delta}$, respectively, while $\bar{\omega}$ and $\bar{\rho}$ are the time components of the isoscalar and isovector vector mean fields. In Eq. (2) the coupling strength of the ω meson is dependent on the number of nonstrange quarks such that $g_\omega^f = (1 + S/3)g_\omega$, with S being the strangeness of f flavor baryon. The strange quark does not carry isospin and as such $g_\rho^f = g_\rho$ since the weighting is carried by I_m^f, the isospin projection. g_ω and g_ρ are the coupling constants for the $\omega - N$ and $\rho - N$ respectively. A similar notation for the σ and δ mesons will be used in Eq. (3). The effective mass in Eq. (1) may be expressed in terms of the scalar fields as follows:

$$\begin{aligned} M_f^*(\bar{\sigma},\bar{\delta}) &= M_f - w_\sigma^f g_\sigma \bar{\sigma} + \tilde{w}_\sigma^f \frac{d}{2}(g_\sigma\bar{\sigma})^2 \\ &\quad - t_\delta^f g_\delta I_m^f \bar{\delta} + \tilde{d} g_\sigma g_\delta \bar{\sigma} I_m^f \bar{\delta} \\ &= M_f - g_\sigma^f(\bar{\sigma})\bar{\sigma} - g_\delta^f(\bar{\sigma}) I_m^f \bar{\delta}. \end{aligned} \quad (3)$$

The scalar polarizabilities (d and $\tilde{d}$) and the flavor dependent weights (w_σ^f, $\tilde{w}_\sigma^f$, and t_δ^f) are calculated using the underlying bag model over a range of densities and involve no new parameters. These reflect the self-consistent response of the internal structure of the bound baryons to the applied scalar fields. The scalar polarizabilities are the origin of the repulsive three-body forces which arise naturally within the model [33,40]. Finally the coupling strengths for the nucleon, calculated in free space using the MIT bag model, are denoted g_σ and g_δ for the $\sigma - N$ and $\delta - N$, respectively. The scalar fields change the effective mass [see Eq. (3)] and the vector fields shift the energy of the baryon [see Eq. (2)].

In the mean field approximation each of the meson field operators is set to its expectation value, while the corrections are treated as a small perturbation, $\sigma \to \langle\bar{\sigma}\rangle + \Delta\sigma$. The integrals range from 0 to the relevant Fermi momentum

$$k_f(n_f) = \sqrt[3]{3\pi^2 n_f}. \quad (4)$$

Omitting the arguments for the Fermi momentum and the effective mass, the meson fields are then

$$m_\sigma{}^2\bar{\sigma} = -2\sum_f \frac{\partial M_f^*}{\partial\bar{\sigma}} \int^{k_f} \frac{d^3k}{(2\pi)^3} \frac{M_f^*}{\sqrt{\vec{k}^2 + M_f^{*2}}}, \quad (5)$$

$$m_\omega{}^2\bar{\omega} = \sum_f g_\omega^f n_f, \quad (6)$$

$$m_\rho{}^2\bar{\rho} = \sum_f g_\rho I_m^f n_f, \quad (7)$$

$$m_\delta{}^2\bar{\delta} = -2\sum_f \frac{\partial M_f^*}{\partial\bar{\delta}} \int^{k_f} \frac{d^3k}{(2\pi)^3} \frac{M_f^*}{\sqrt{\vec{k}^2 + M_f^{*2}}}. \quad (8)$$

The contribution to the energy density from baryons and the meson fields, ϵ_B, is

$$\epsilon_B = \frac{\langle\mathcal{H}_B + \mathcal{V}_\sigma + \mathcal{V}_\omega + \mathcal{V}_\rho + \mathcal{V}_\delta + \mathcal{V}_\pi\rangle}{V}. \quad (9)$$

In the Hartree-Fock approximation, all meson exchanges are evaluated as follows:

$$\frac{\langle\mathcal{H}_B\rangle}{V} = 2\sum_f \int^{k_f} \frac{d^3k}{(2\pi)^3}\sqrt{\vec{k}^2 + M_f^{*2}}, \quad (10)$$

$$\frac{\langle\mathcal{V}_\sigma\rangle}{V} = \frac{m_\sigma{}^2\bar{\sigma}^2}{2} + \frac{\lambda_3}{3!} g_\sigma{}^3\bar{\sigma}^3 + \sum_f \left(\frac{\partial M_f^*}{\partial\bar{\sigma}}\right)^2 \int^{k_f}\int^{k_f} \frac{d^3k_1 d^3k_2}{(2\pi)^6} \frac{1}{(\vec{k}_1 - \vec{k}_2)^2 + m_\sigma{}^2} \frac{M_f^{*2}}{\sqrt{\vec{k}_1^2 + M_f^{*2}}\sqrt{\vec{k}_2^2 + M_f^{*2}}}, \quad (11)$$

$$\frac{\langle \mathcal{V}_\omega \rangle}{V} = \frac{{m_\omega}^2 \bar{\omega}^2}{2} - \sum_f {g_\omega^f}^2 \int^{k_f} \int^{k_f} \frac{d^3k_1 d^3k_2}{(2\pi)^6} \frac{1}{(\vec{k}_1 - \vec{k}_2)^2 + {m_\omega}^2}, \tag{12}$$

$$\frac{\langle \mathcal{V}_\rho \rangle}{V} = \frac{{m_\rho}^2 \bar{\rho}^2}{2} - \sum_{f,f'} {g_\rho}^2 \int^{k_f} \int^{k'_f} \frac{d^3k_1 d^3k_2}{(2\pi)^6} \frac{C_{m,m'}\delta_{S,S'}}{(\vec{k}_1 - \vec{k}_2)^2 + {m_\rho}^2}, \tag{13}$$

$$\frac{\langle \mathcal{V}_\delta \rangle}{V} = \frac{{m_\delta}^2 \bar{\delta}^2}{2} + \sum_{f,f'} \left(g_\delta^f(\bar{\sigma}) g_\delta^{f'}(\bar{\sigma}) \right) \int^{k_f} \int^{k'_f} \frac{d^3k_1 d^3k_2}{(2\pi)^6} \frac{C_{m,m'}\delta_{S,S'}}{(\vec{k}_1 - \vec{k}_2)^2 + {m_\delta}^2} \frac{M_f^*}{\sqrt{\vec{k}_1^2 + {M_f^*}^2}} \frac{M_{f'}^*}{\sqrt{\vec{k}_2^2 + {M_{f'}^*}^2}}. \tag{14}$$

Equation (11) includes the term cubic in the σ field required to lower the incompressibility of symmetric nuclear matter sufficiently to yield acceptable GMR energies. The strength of the self-interaction is governed by the coefficient λ_3. The solutions of Eqs. (12) and (13) are simple to evaluate, because they correspond to two-body interactions. Equations (11) and (14) are more complicated, because the σ and δ mean fields are functions of M_f^*, which in turn depend on σ and δ. These are solved self-consistently at β equilibrium for each given number density (see Stone *et al.* [34]). The notation for $C_{m,m'}$ is given in Eq. (15) and is expressed in terms of the Kronecker delta ($\delta_{m,m'}$), the isospin (I_t^f), and its projection (I_m^f), consistent with Ref. [39]. Each baryon flavour f has an associated S, t, and m corresponding to the strangeness, isospin, and projection respectively. Equations (13) and (14) involve double summation and are only nonzero when $S = S'$ ($\delta_{S,S'}$). In Eq. (14) we have used the fact that $\frac{\partial M_f^*}{\partial \delta} = -g_\delta^f(\bar{\sigma}) I_m^f$ and allow $C_{m,m'}$ to carry the isospin dependence,

$$C_{m,m'} = \delta_{m,m'} {I_m^f}^2 + (\delta_{m,m'+1} + \delta_{m+1,m'}) I_t^f. \tag{15}$$

While we have used a nonrelativistic approximation to the Fock terms in Eqs. (11) to (14), rather than the relativistic form used in earlier work [57], this has no bearing on the effect of the overlap term which is the focus of the present study.

Finally the long-range pion Fock terms [34,58] are

$$\frac{\langle \mathcal{V}_\pi \rangle}{V} = \left(\frac{g_A}{2f_\pi} \right)^2 \Big\{ J_{pp} + 4J_{pn} + J_{nn} + \frac{1}{25}(J_{\Xi^-\Xi^-} + 4J_{\Xi^-\Xi^0} + J_{\Xi^0\Xi^0}) \Big\}, \tag{16}$$

where

$$J_{ff'} = \int^{k_f} \int^{k'_f} \frac{d^3k_1 d^3k_2}{(2\pi)^6} \left[1 - \frac{{m_\pi}^2}{(\vec{k}_1 - \vec{k}_2)^2 + {m_\pi}^2} \right] \tag{17}$$

and the δ function associated with the first term in the square brackets is dropped because of short distance repulsion. Note that parameters in Eqs. (16) and (17) are set to $m_\pi = 139$ MeV, $g_A = 1.26$, and $f_\pi = 93$ MeV [40].

The phenomenological bag overlap term, denoted $\mathcal{H}_O$, is approximated by a simple Gaussian wave function, with the overall strength E_0 and range b treated as free parameters, subject to the constraint that this term must not change nuclear matter properties at saturation density:

$$\frac{\langle \mathcal{H}_O \rangle}{V} = E_0 n_B \exp\left\{ -\left(\frac{n_B^{-1/3}}{b} \right)^2 \right\}. \tag{18}$$

We note that $n_B^{-1/3}$ is roughly the average distance between baryons in a Fermi gas. Given that b characterizes the size of the quark cores of the baryons, we expect it to be of order 0.5 fm. This additional term is added to Eq. (9). The overlap term is assumed independent of the quark content of the baryon and is repulsive. This concludes the construction of the energy density for nuclear matter within the QMC framework.

B. β equilibrium

The material in the NS is assumed to be cold and in β equilibrium. Any particulate species which exist longer than the timescale of the system then participate to minimize the energy density. This includes the hyperons which are stable at high densities, because of Pauli blocking. The total energy density of the system, including the leptons (electron and muon), is minimized under the condition of β equilibrium. Thus the total energy density is

$$\epsilon_{\text{total}} = \epsilon_B + \epsilon_e(n_e) + \epsilon_\mu(n_\mu), \tag{19}$$

where ϵ_B is given by Eqs. (9) and (18). The energy density of the electrons and muons is described by a free gas of leptons:

$$\epsilon_l(n_l) = 2 \int^{k_l(n_l)} \frac{d^3k}{(2\pi)^3} \sqrt{\vec{k}^2 + {m_l}^2}, \tag{20}$$

where $k_l(n_l)$ is given by Eq. (4).

Charge neutrality is imposed along with conservation of baryon number. The equilibrium condition is then given by Eq. (21), shown below [34]:

$$\delta \Big\{ \epsilon_B(n_n, n_p, n_\Lambda, n_{\Xi^0}, n_{\Xi^-}) + \epsilon_e(n_e) + \epsilon_\mu(n_\mu) + \Lambda_1 \sum_i n_i q_i + \Lambda_2 \left(\sum_f n_f - n_B \right) \Big\} = 0. \tag{21}$$

Here Λ_i are Lagrange multipliers. The electrical charge is denoted by q_i with the summation over the baryons and the leptons.

III. RESULTS

The EoS generated by the QMC model supplemented by the phenomenological overlap term [Eq. (18)] will be studied either with or without the term cubic in the σ field. The strength of σ^3 is determined by the coefficient λ_3, which is chosen to be $\lambda_3 = 0.02$ fm^{-1} or $\lambda_3 = 0$ fm^{-1}. The choice $\lambda_3 = 0.02$ fm^{-1} is motivated by the study of the energies of GMR by Martinez *et al.* [41], where it was found that this was the smallest value of λ_3 capable of producing a value for the nuclear incompressibility compatible with that data. Where the overlap term is explicitly included, the EoS will be denoted by *overlap*. When it is not included the EoS will be denoted *no overlap*. If the derived EoS includes hyperons, then it will be denoted *F-QMC*, while the case where only nucleons are included will be denoted *N-QMC* as a comparison.

Given that the inclusion of $\lambda_3 = 0.02$ fm^{-1} leads to a maximum NS mass that is unacceptably low when hyperons are included, various overlap parameters (E_0 and b) were explored:

(i) Overlap energy: $E_0 = 3500, 4500, 5500$ MeV.
(ii) Range parameter: $b = 0.4, 0.5$ fm.

The upper limits on both the overlap energy and range parameter were set by the requirement that there be no significant change in the properties of symmetric nuclear matter at saturation density. Where the parameters are left unspecified in what follows, they were chosen to be $E_0 = 5500$ MeV and $b = 0.5$ fm. These are the preferred choice, in that they lead to an acceptable maximum mass while not altering the nuclear matter parameters.

The bulk properties of the NS are used to test the viability of the model at high density. The properties of interest are the mass-radius relationship and the tidal deformability. For brevity, only PSR J0740+6620 is shown when constraining the QMC EoS. The mass is taken to be $M = 2.072^{+0.067}_{-0.066} M_\odot$, with a 68% interval around the median [21,22]. GW170817 serves as a constraint for the tidal deformability, Λ_M [24].

A. The choice of parameters

The mass of the σ meson is set at 700 MeV, while the masses of the other mesons are taken from their experimental values ($m_\delta = 983$ MeV, $m_\rho = 770$ MeV, $m_\omega = 783$ MeV). In terms of these masses the meson-nucleon coupling strengths in free space are often written as

$$G_\sigma = \frac{{g_\sigma}^2}{{m_\sigma}^2}, \quad G_\omega = \frac{{g_\omega}^2}{{m_\omega}^2}, \quad G_\rho = \frac{{g_\rho}^2}{{m_\rho}^2}. \tag{22}$$

$G_\delta = 3$ fm^2 is chosen as the preferred value for the coupling of the δ field [39,59] but, for comparison, in the Appendix all calculations are repeated for $G_\delta = 0$ fm^2.

In all cases (with and without λ_3 and G_δ) we require that the bag overlap terms do not alter the properties of nuclear matter at saturation density. The couplings are fixed at the typical values $n_0 = 0.16$ fm^{-3}, the binding energy per nucleon at n_0 is taken to be $E_B/A = -15.8$ MeV, while the symmetry energy is $S = 30$ MeV [1,2,60]. The couplings are specified without the overlap term and held fixed when the overlap is introduced. The incompressibility and the slope of the symmetry energy are typically taken to lie in the ranges $K_\infty = 250 \pm 50$ MeV [61,62] and $L_0 = 60 \pm 20$ MeV [60]. We choose to use $K_\infty = 260$ MeV and $L_0 = 62$ MeV respectively, because, while the relation between the incompressibility and the energies of the GMR is somewhat complicated [63,64], calculations of the GMR using the QMC EDF tend to favor values of K_∞ at the lower end of this range [61].

As reported by Guichon *et al.* [40], the inclusion of $\lambda_3 = 0.02$ fm^{-1} lowers K_∞ by about 10%, leading to the value 260 MeV noted earlier. This remains unchanged for $b = 0.4$ fm for E_0 ranging from 3500 to 5500 MeV, while it increases slightly (from 262 to 264 MeV) over this range of E_0 for $b = 0.5$ fm. So long as $b < 0.6$ fm then $K_\infty < 300$ MeV is within the acceptable limits. On the other hand, for $\lambda_3 = 0$ fm^{-1} the incompressibility is 295 MeV (rising to 298 MeV for $b = 0.5$ fm). Physically the range parameter sets the scale at which the extra repulsive force acts in medium. Since saturation density is relatively low, the overlap term has essentially no influence there and thus does not affect the properties of finite nuclei. In NSs, the gravitational force compacts the baryonic matter well past saturation, allowing them to eventually overlap [15]. The extra repulsion induced by baryon overlap stiffens the EoS at supranuclear densities. This is explored in Sec. III C.

B. NS composition under β equilibrium

Within the QMC model it was previously demonstrated [38,57] that among the hyperons only the Λ and $\Xi^{0,-}$ appear. It is worth noting at this point that the omission of any coupling of the mesons to the s quark produces surprisingly good results for Λ hypernuclei [56] as well as the extremely limited data on Ξ hypernuclei [65]. It has long been established that Σ hyperons experience a repulsive interaction in nuclear matter [66], and this is indeed found in the QMC model. It is then not surprising that Σ hyperons were not found in earlier work on NS using the QMC model [67], which is why they are simply omitted here. The physical reason underlying this result is the enhancement of the color hyperfine interaction in medium [56] and the repulsive three-body force generated by the scalar polarizability. This means that the $\Sigma^{\pm,0}$ baryons experience significant repulsion and are not energetically allowed at densities $n_B \leqslant 1.2$ fm^{-3}.

The species fractions inside a NS, as predicted by F-QMC, are shown in Fig. 1. F-QMC predicts no hyperons below $3n_0$. The overlap term has no bearing on the species fraction because the repulsion introduced by the overlap is independent of quark content and hence minimization of the energy density is not affected. There is a difference in the appearance of hyperons with (solid) and without (dashed) λ_3. The $\Xi^{0,-}$ appears slightly later when the term in σ^3 is present. The relative abundances are also modified.

Table I lists the chemical potentials of the baryon species, with and without overlap ($E_0 = 5500$ MeV and $b = 0.5$ fm), calculated at saturation density. The overlap term increases chemical potentials for all baryon species, but, since Table I is measured at low densities, the effect is negligible. We see that the Λ experiences an attractive potential of 35–40 MeV, while the attraction felt by the Ξ^0 is considerably smaller. These

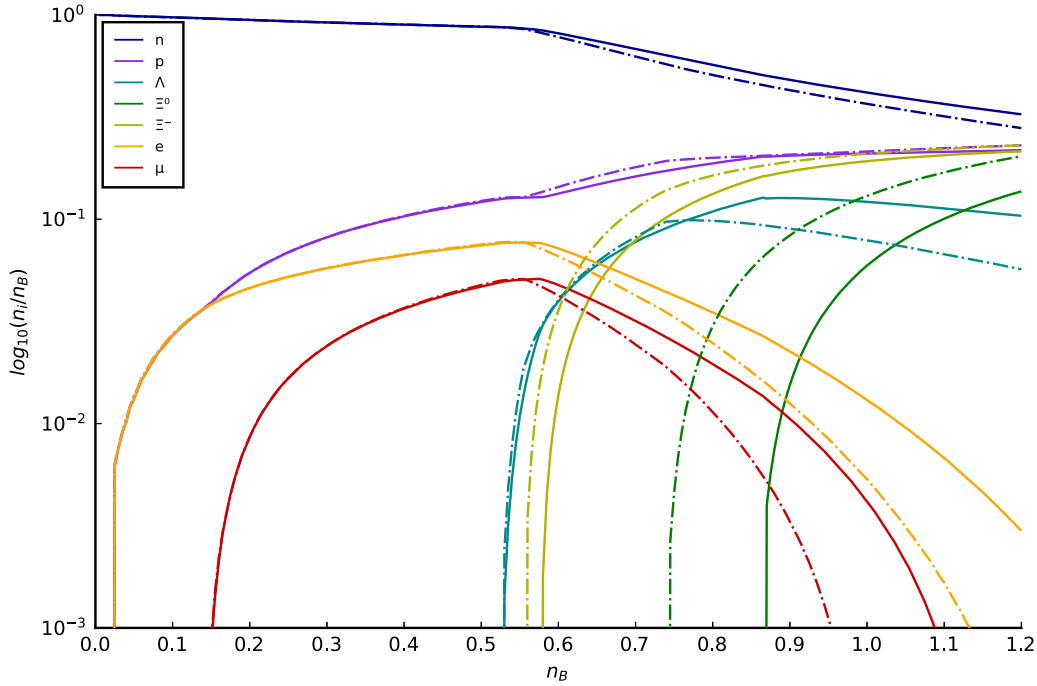

FIG. 1. β-equilibrium was calculated for $0 < n_B < 1.2$ fm^{-3}. Species fractions of the nucleons, leptons, and hyperons are shown relative to the total baryon number, n_B, for F-QMC with overlap. Solid lines indicate $\lambda_3 = 0.02$ fm^{-1}, while the dashed lines are for the case $\lambda_3 = 0$ fm^{-1}. Not shown are the curves for F-QMC without overlap, as they have identical species fractions.

values are consistent with the fact that the Λ is bound in the $1s$ state in Pb by around 26 MeV [68], as well as with the recent observation of a Ξ weakly bound to ^{14}N [56,65,69].

C. QMC EoS

The low density crustal region enveloping the core of a NS is populated by nuclei with increasing neutron excess [70–72]. Here the QMC EoS, which is an appropriate description of nuclear matter, is matched onto the low density EoS provided by Hempel and Schaffner-Bielich [73,74]. The Hempel and Schaffner-Bielich model is a relativistic mean field model for interacting nucleons which takes into account excluded volume effects. In what follows the QMC EoS is matched to the crust region at $n \approx 0.7 n_0$, which is appropriate in describing the transition of nuclei to nuclear matter at the crust-core boundary.

The derived F-QMC (solid) and N-QMC (dashed) EoSs, with crust, are shown in Fig. 2. Note that in all figures, unless otherwise stated, the overlap case corresponds to $b = 0.5$ fm and $E_0 = 5500$ MeV. As expected, the hyperons soften the EoS when compared to that for nucleons only. While the inclusion of the overlap term has no influence on the nuclear matter parameters at saturation density, it is clear that the EoS is significantly stiffer at high density. In Fig. 2 we see that the effect of the overlap term becomes considerable at energy densities of order 250–350 MeV fm^{-3}, or $n_B > 2n_0$. Furthermore, the degree of softening induced by the hyperons is reduced at higher densities. Comparing the two panels in Fig. 2, the cubic term in $V(\sigma)$ [see Fig. 2(a)], acts to soften the EoS, whether hyperons are included or not.

TABLE I. The chemical potentials, μ_i in MeV, for each baryon at saturation density, with and without overlap.

F-QMC	n	p	Λ	Ξ^0	Ξ^-
			$\lambda_3 = 0.02$ fm^{-1}		
Overlap	970	857	1076	1300	1326
No overlap	970	857	1076	1300	1326
			$\lambda_3 = 0$ fm^{-1}		
Overlap	970	856	1080	1298	1333
No overlap	970	856	1080	1298	1333

In order to make the QMC EoS generated here (without crust) widely available, an analytic function has been fitted to the F-QMC with overlap EoS for $\lambda_3 = 0.02$ fm^{-1} and $\lambda_3 = 0$ fm^{-1}. This is valid for the energy density range 0–1600 MeV fm^{-3} but must be matched to a crust EoS for $n < 0.7 n_0$, corresponding to an energy density $\epsilon \approx 105$ MeV fm^{-3}. Equation (23) takes the argument for energy density in MeV fm^{-3} and gives the pressure in MeV fm^{-3}:

$$P(\epsilon) = N_1 \epsilon^{p_1} + N_2 \epsilon^{-p_2}. \tag{23}$$

The error computed is given by

$$\text{RMSE}\ (\%) = \sqrt{\frac{1}{N}\sum_i^N \frac{(x_i - y_i)^2}{{y_i}^2}} \times 100, \tag{24}$$

and the parameters are summarized in Table II, with the energy density split into different regions. The relative mean squared error (RMSE) estimates the difference between the model's prediction (x_i), as cited in Eq. (23), and that theorized by QMC (y_i). Equation (23) is not suitable for

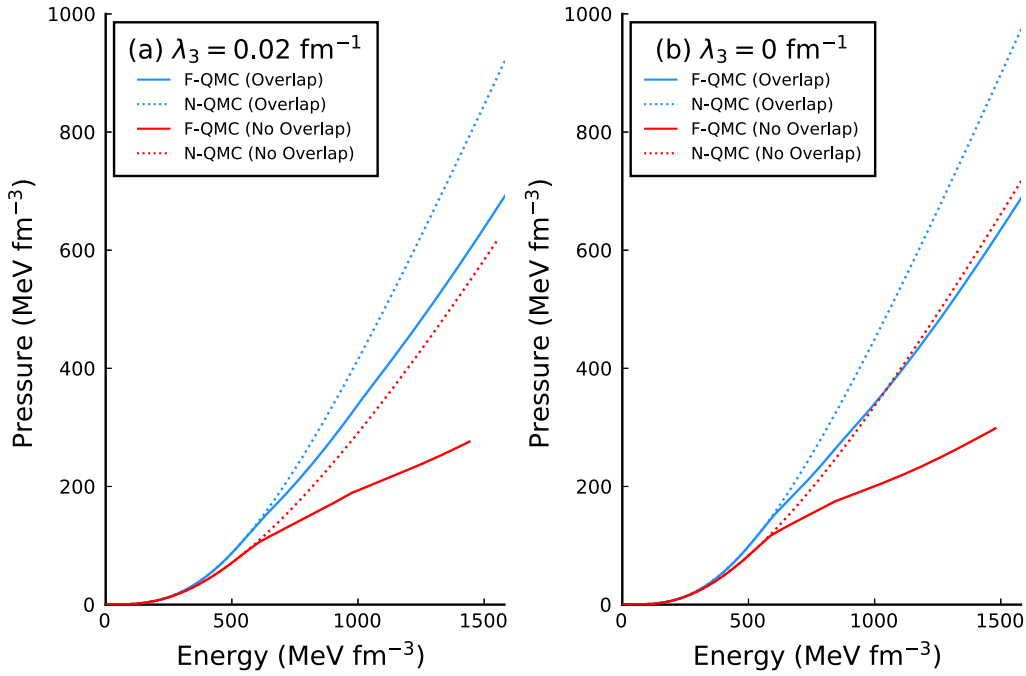

FIG. 2. The EoS for the models considered here, where N-QMC includes only nucleons and F-QMC includes hyperons. (a) corresponds to $\lambda_3 = 0.02$ fm^{-1}, whilst the right panel (b) is $\lambda_3 = 0$ fm^{-1}.

computing the speed of sound [Eq. (29)] as the domain boundaries do not precisely correspond to the appearance of new species.

D. NS bulk properties

The Tolman-Oppenheimer-Volkoff (TOV) equation was used to compute the mass and radius of the NS. Assuming that the NS is nonrotating and spherically symmetric, the TOV equation is

$$\frac{dp}{dr} = -\frac{[p(r)+\epsilon(r)][M(r)+4\pi r^3 p(r)]}{r[r-2M(r)]}, \tag{25}$$

where

$$M(r) = 4\pi \int_0^r \epsilon(r')(r')^2 dr'. \tag{26}$$

TABLE II. Parameters for Eq. (23), corresponding to the F-QMC with overlap EoS for $\lambda_3 = 0.02$ fm^{-1} and $\lambda_3 = 0$ fm^{-1}. The domains for the energy density, ϵ (MeV fm^{-3}), have been split as denoted by the left-hand column.

ϵ	N_1	p_1	N_2	p_2	RMSE
		F-QMC with $\lambda_3 = 0.02$ fm^{-1}			
0–34	7.733×10^{-4}	1.203			1.49%
35–90	6.171×10^{-7}	3.043	1.578	1.128	0.64%
91–133	3.309×10^{-7}	3.186			0.10%
134–298	1.260×10^{-6}	2.921			1.09%
299–550	5.884×10^{-6}	2.656			1.16%
551–620	8.387×10^{-5}	2.234			0.13%
621–1021	1.730×10^{-3}	1.764			0.10%
1022–1600	8.269×10^{-3}	1.539			0.11%
		F-QMC with $\lambda_3 = 0$ fm^{-1}			
0–24	9.725×10^{-4}	1.183			4.04%
25–90	6.234×10^{-8}	3.498	1.549×10^{-2}	−0.3064	1.10%
91–162	1.376×10^{-7}	3.355			0.66%
163–299	6.243×10^{-7}	3.064			1.02%
300–549	7.150×10^{-6}	2.645			1.59%
550–595	1.143×10^{-4}	2.204			0.06%
596–861	4.517×10^{-3}	1.629			0.05%
862–1600	8.295×10^{-3}	1.538			0.25%

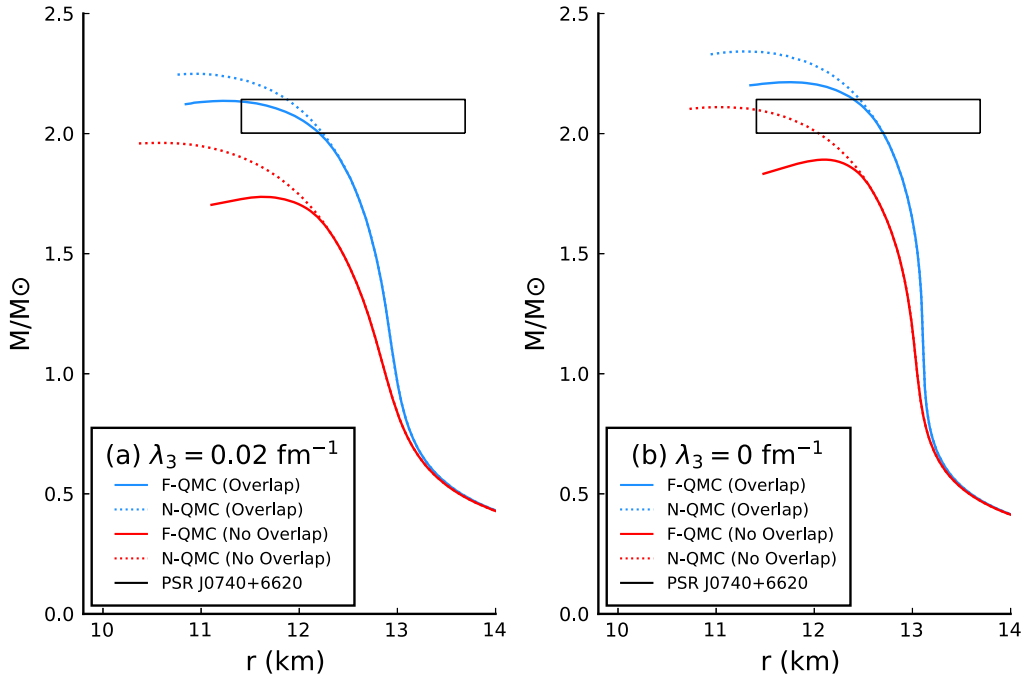

FIG. 3. The mass-radius sequence of stars computed from QMC EoS shown in Fig. 2. The box constraint (black) is PSR J0740+6620, extracted from Ref. [21]. In (a) $\lambda_3 = 0.02$ fm^{-1} and has a reduced maximum mass compared to (b) when $\lambda_3 = 0$ fm^{-1}.

The central pressure is chosen at $r = 0$ and integrated outwards until $p(R) = 0$, where R is the final radius of the star. This process is repeated for different central pressures to form the sequence of stars plotted in Fig. 3. The box denotes the constraint corresponding to pulsar PSR J0740+6620, $M = 2.072^{+0.067}_{-0.066}\,M_\odot$ and $R = 12.39^{+1.30}_{-0.98}$ km. The total baryon number is given by

$$A = \int_0^R \frac{4\pi r^2 n_B(r)}{\left(1 - \frac{2GM(r)}{r}\right)^{\frac{1}{2}}} dr. \tag{27}$$

GW 170817 is a binary system with a total mass of $2.73^{+0.04}_{-0.01}\,M_\odot$ [24]. The component masses in the low spin case are $m_1 \in [1.18, 1.36]\,M_\odot$ and $m_2 \in [1.36, 1.58]\,M_\odot$. The tidal deformability may be computed as

$$\Lambda_M = \frac{2}{3} k_2 \left(\frac{R}{M}\right)^5. \tag{28}$$

The dimensionless constant, k_2, is the tidal Love number and the full equation is given in Refs. [27,75]. Equation (28) gives the one-sided tidal deformation, which is constrained by GW170817 for a $1.4M_\odot$ star to lie in the range $\Lambda_{1.4} = 190^{+390}_{-120}$ [24]. This is shown as a black line in Fig. 4. However, we note that other work has reported that the upper limit on $\Lambda_{1.4}$ could be as large as 800 [76].

1. Mass-radius relation

Table III summarizes the properties of a NS with maximum mass, $M_{\max}$, predicted by QMC. All entries are for the case where hyperons are included, unless otherwise indicated. The overlap parameters alter the NS properties in predictable ways. Increasing E_0 has mild effects on the maximum mass of the star, with little change to its radius. The range parameter

TABLE III. Macroscopic properties of the NS (including hyperons unless otherwise indicated) are computed with variations of the overlap parameters. The range parameter b and overlap energy E_0 have units of fm and MeV, respectively. The results summarize the maximum mass ($M_{\max}$, $M_\odot$), total baryon number (A, 10^{57}) and central number density (n_c, fm^{-3}), central pressure (P_c, MeV fm^{-3}), and central energy density (ϵ_c, MeV fm^{-3}) for each parameter set used.

b	E_0	$M_{\max}$	A	n_c	P_c	ϵ_c
			$\lambda_3 = 0.02$ fm^{-1}			
0.4	3500	1.77	2.41	1.01	256	1191
0.4	4500	1.78	2.43	1.02	268	1205
0.4	5500	1.79	2.45	1.03	280	1219
0.5	3500	2.02	2.82	1.02	408	1260
0.5	4500	2.08	2.92	1.01	448	1258
0.5	5500	2.14	3.02	1.00	492	1267
0.5[a]	5500	2.25	3.22	1.00	680	1314
[b]	0	1.74	2.36	0.961	213	1111
[c]	0	1.96	2.74	1.15	559	1461
			$\lambda_3 = 0$ fm^{-1}			
0.4	3500	1.91	2.63	0.883	221	1030
0.4	4500	1.92	2.64	0.900	231	1055
0.4	5500	1.92	2.65	0.915	242	1078
0.5	3500	2.11	2.97	0.906	336	1102
0.5	4500	2.17	3.05	0.923	387	1144
0.5	5500	2.21	3.14	0.903	406	1123
0.5	5500	2.34	3.37	0.934	643	1222
	0	1.89	2.60	0.867	201	1005
	0	2.11	2.97	1.03	529	1305

[a]N-QMC (overlap).
[b]F-QMC (no overlap).
[c]N-QMC (no overlap).

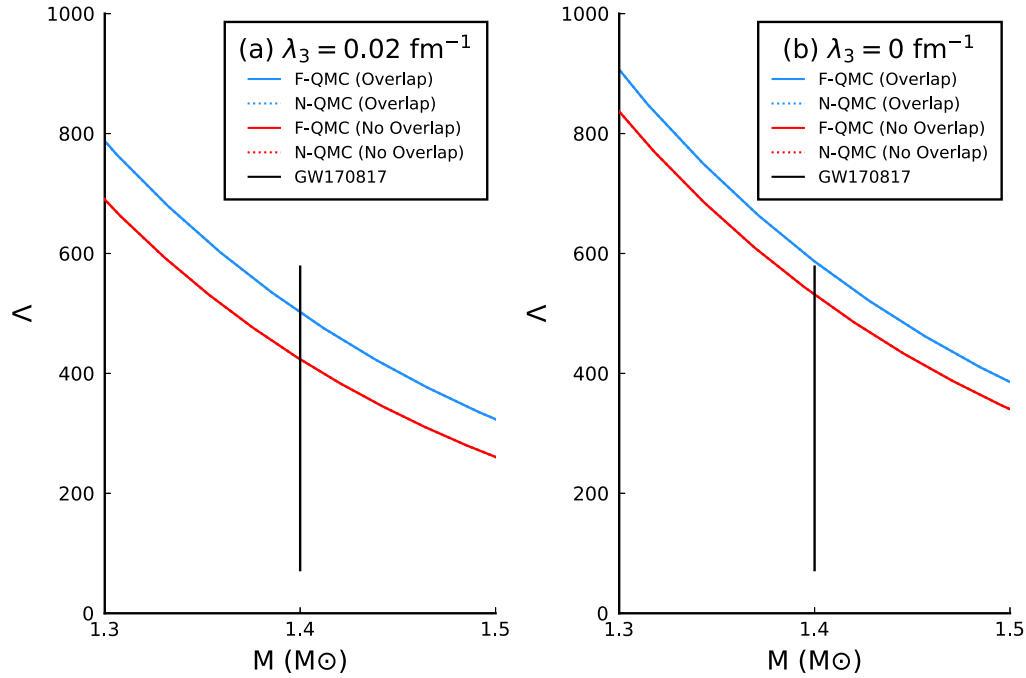

FIG. 4. Tidal deformability for the QMC EoS when (a) $\lambda_3 = 0.02$ fm^{-1} and (b) $\lambda_3 = 0$ fm^{-1}. Given that no hyperons appear in a star of mass $1.4M_\odot$ the solid (F-QMC) and dashed (N-QMC) lines are superimposed. GW170817 is shown by the solid black line and extracted from [24].

b, however, raises the mass substantially as it is increased. For $b = 0.4$ fm and $\lambda_3 = 0.02$ fm^{-1}, the maximum mass is predicted to be $M_{\rm max} < 2M_\odot$, which is unsatisfactory.

Table IV reflects the central properties of different mass NSs predicted for F-QMC with overlap. The central density, pressure, and energy densities are all greater when $\lambda_3 = 0.02$ fm^{-1}, for all masses. For a star of mass $M = 1.4M_\odot$, the number density is lower than the threshold density for hyperons and hence there are no hyperons in these stars. However, as the density increases the star's core is then populated by hyperonic matter.

TABLE IV. The central number density (n_c, fm^{-3}), pressure (P_c, MeV fm^{-3}) and energy density (ϵ_c, MeV fm^{-3}) for different mass stars ($M_\odot$) predicted by F-QMC with overlap ($E_0 = 5500$ MeV, $b = 0.5$ fm).

Mass	n_c	P_c	ϵ_c
		$\lambda_3 = 0.02$ fm^{-1}	
1.0	0.341	30	336
1.4	0.427	59	432
1.6	0.482	86	496
1.8	0.547	124	576
2.0	0.663	196	733
		$\lambda_3 = 0$ fm^{-1}	
1.0	0.317	27	311
1.4	0.395	53	397
1.6	0.438	74	447
1.8	0.487	102	507
2.0	0.564	154	607

In Fig. 3, the mass-radius curve shows that the overlap term is essential in predicting a heavy NS, $M > 2M_\odot$, once the incompressibility is reduced to the preferred range [i.e., with $\lambda_3 = 0.02$ fm^{-1} in Fig. 3(a)]. Without the overlap term, the mass of the star is significantly lower. The inclusion of the σ^3 term acts to reduce the radius and lower the star's mass. The mass reduction is caused by the additional scalar meson attraction, with a consequent softening of the EoS. For $\lambda_3 = 0.02$ fm^{-1}, the radius of the star slightly increases as the mass decreases from $1.5M_\odot$ to $1.0M_\odot$, in contrast to the case $\lambda_3 = 0$ fm^{-1}, where there are no significant changes to the radius. In the phenomenologically interesting region, $M \approx 1.4M_\odot$, the radius of the star is significantly lower when $\lambda_3 = 0.02$ fm^{-1}.

The presence of hyperons reduces the maximum mass, as well as increasing the radius at maximum mass. From Fig. 3 we see that the overlap term decreases the radius at maximum mass for F-QMC, whereas for N-QMC the radius is increased at maximum mass when the overlap term is present.

Figure 4 illustrates the tidal deformability for the QMC EoS. The dashed line for the nucleon only case cannot be distinguished from F-QMC because the QMC model predicts no hyperons in a $1.4M_\odot$ star. For $\lambda_3 = 0.02$ fm^{-1} the tidal deformation is acceptable with and without overlap. The introduction of the overlap term does causes an increase in the radius around the canonical mass, and this in turn increases the tidal deformability.

E. Speed of sound

In the absence of direct observations of the composition of the core of a NS, theoretical calculations of the speed of sound

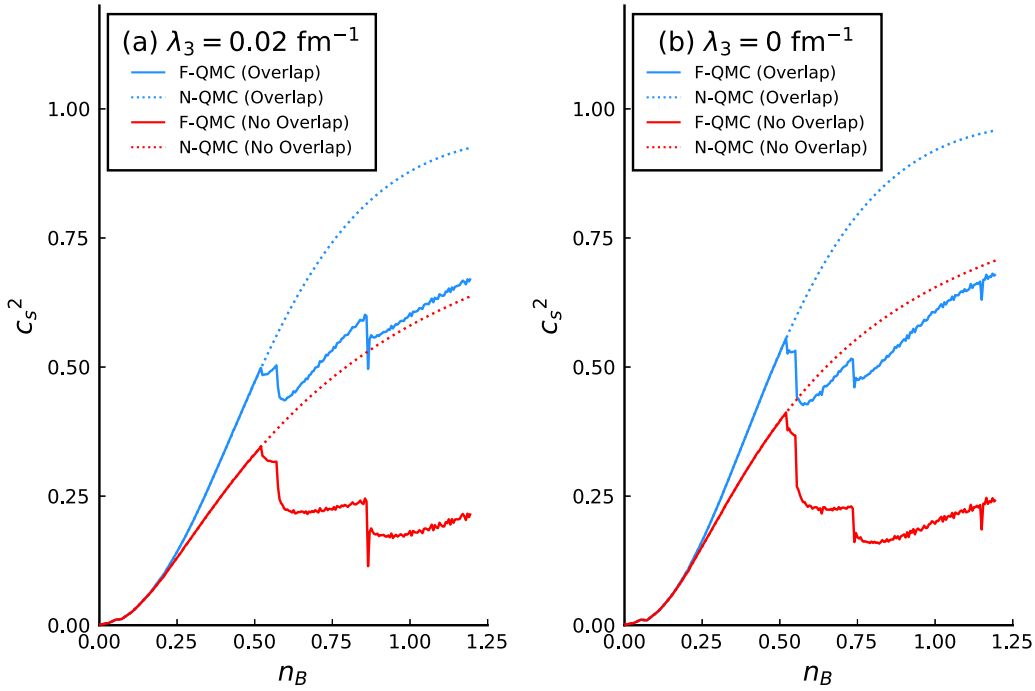

FIG. 5. The speed of sound (c_s^2) is given as a fraction of the speed of light for (a) $\lambda_3 = 0.02$ fm^{-1} and (b) $\lambda_3 = 0$ fm^{-1}. The number density n_B is given in fm^{-3}. Nontrivial drops in c_s^2 correspond to the initial appearance of hyperons (see Fig. 1).

(equivalently, polytropic index γ) do offer valuable insights. It has previously been suggested that nontrivial changes in the EoS correspond to phase changes from hadronic matter to either quark matter [6] or the threshold of creation of hyperons [37].

The EoSs at low and extremely high densities have been extensively studied in effective field theory ($n_B < 1.1n_0$) and perturbative QCD ($n_B > 40n_0$), respectively. Annala *et al.* [6] suggest that, for stars with $M = 1.4M_\odot$, hadronic nuclear theories are suitable in predicting the EoS giving rise to canonical mass stars. The QMC model is consistent with their EoS in that region. However, for $M > 2M_\odot$, Annala *et al.* suggest that the central density becomes so large that the cores of the stars may be populated by deconfined quark matter and gluons [6]. Quark matter, being conformal and scale invariant, would then have a speed of sound, $c_s^2 = \frac{1}{3}$, approaching logarithmically from below as the density increases. On the other hand, it has been shown that this is not a distinct feature of conformal matter [37,38]. Since the QMC model does not contain any elements of deconfined quarks, $c_s^2 < \frac{1}{3}$ approaching from below, may also be interpreted as the creation of hyperons. Recall that the speed of sound is defined as

$$c_s^2 = \frac{dP}{d\epsilon}. \tag{29}$$

Figure 5 shows the three sudden changes in c_s^2 which occur at those number densities where the different species of hyperons first appear (see Fig. 1). In order of appearance, these are the Λ, Ξ^-, and Ξ^0. Without the overlap term, the results reflect those reported by earlier QMC models [37,38]. However, when the overlap terms are included, c_s^2 can be as large as 0.5 or more. This is consistent with pure hadronic matter, as cited in [6].

IV. CONCLUSION

The excitement of studying neutron stars is that they contain the most dense matter in the Universe. Thus they may be expected to yield insights into the EoS of strongly interacting matter at densities inaccessible in any other way.

Relativistic descriptions of nuclear matter typically lead to higher values of the incompressibility of nuclear matter, K_∞, than nonrelativistic Skyrme forces. While the connection between the incompressibility and the energies of GMR is complex, there is a tendency for lower values of K_∞ to be preferred. The energy density functional derived within the QMC model requires a small cubic term involving the scalar field in order to reproduce the observed GMR energies. This in turn lowers the maximum masses of the neutron stars generated by the model.

In order to solve that problem, we have explored the impact on the EoS of dense matter and the properties of neutron stars by introducing a phenomenological repulsive contribution to the energy density as the degree to which the baryonic overlap increases. This new term is designed such that it does not alter the properties of nuclear matter at saturation density.

The effects of this new overlap term are indeed to generate neutron stars with a maximum mass above $2.1M_\odot$, even when hyperons are included. The radii of stars around $1.4M_\odot$ lie just below 13 km, which is the upper end of the range preferred by the analysis of the gravitational wave data from GW170817.

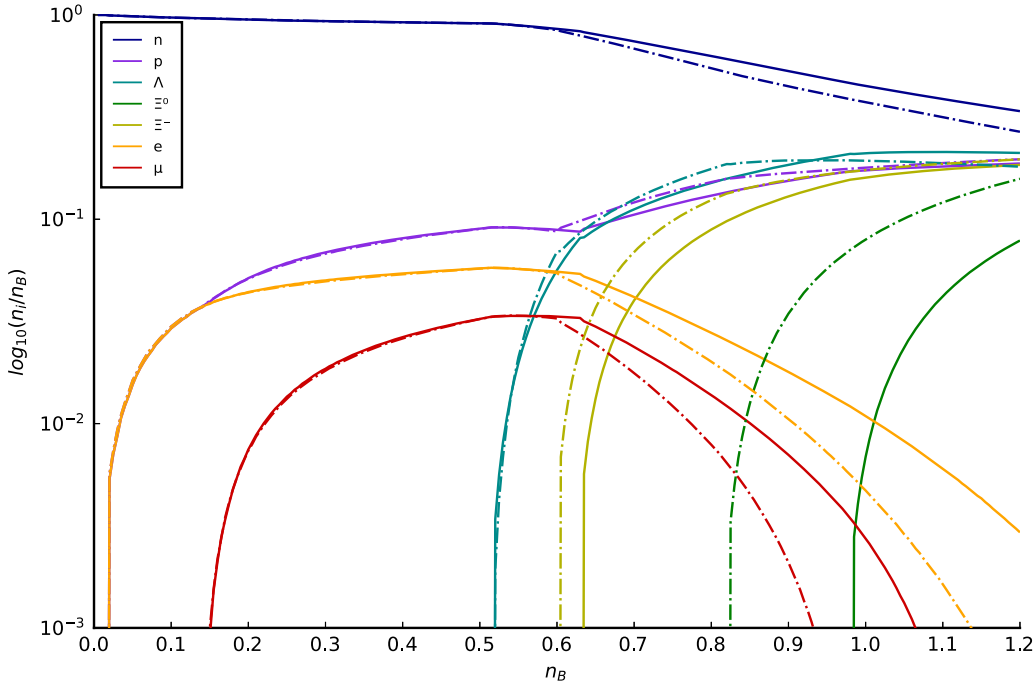

FIG. 6. β-equilibrium was calculated for $0 < n_B < 1.2$ fm^{-3} with $G_\delta = 0$ fm^2. Only the F-QMC with overlap species fraction is shown with the solid line corresponding the $\lambda_3 = 0.02$ fm^{-1} and the dashed line showing the case for $\lambda_3 = 0$ fm^{-1}. The no overlap case is not shown as it produces identical species fractions.

The calculated values of the tidal deformability also lie within the bounds determined from that data. The one qualitative change from earlier work is that in contrast with the values of c_s^2 found with hyperons, which lie below $\frac{1}{3}$, with the overlap term they become as large as 0.6. Such large values are consistent with those expected in hadronic models, in contrast with the lower range anticipated for quark matter.

ACKNOWLEDGMENTS

We are pleased to acknowledge Jirina Stone for a careful reading of this manuscript and a number of helpful comments. This work was supported by the University of Adelaide and the Australian Research Council through a grant to the ARC Centre of Excellence for Dark Matter Particle Physics (CE200100008).

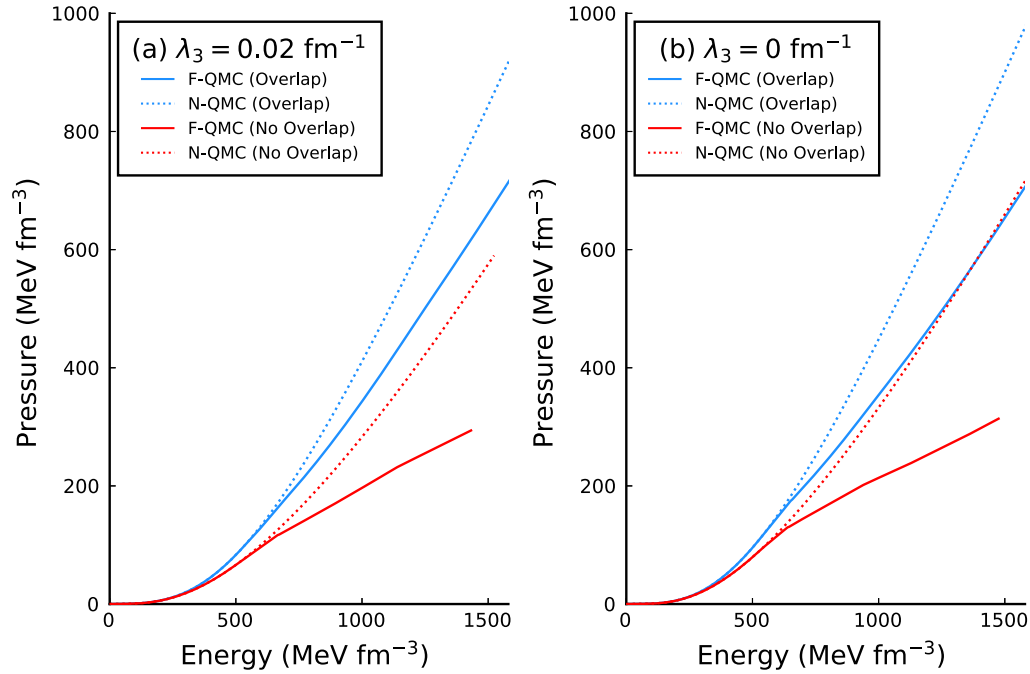

FIG. 7. QMC EoS with $G_\delta = 0$ fm^2 for values of λ_3 as (a) $\lambda_3 = 0.02$ fm^{-1} and (b) $\lambda_3 = 0$ fm^{-1}.

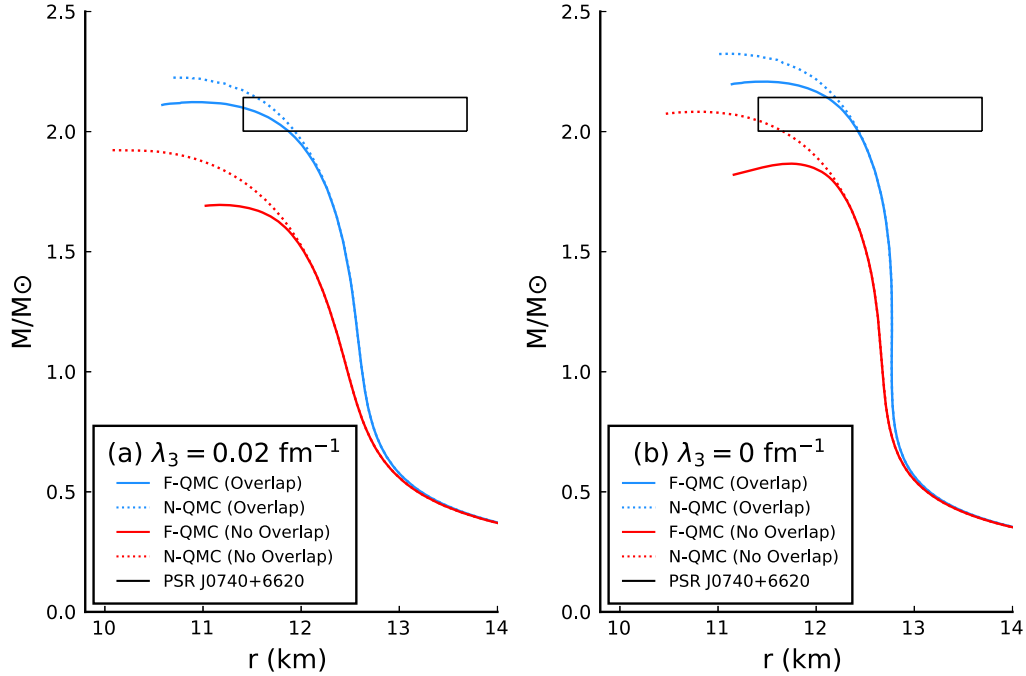

FIG. 8. MR curve for $G_\delta = 0$ fm^2. The left panel is (a) $\lambda_3 = 0.02$ fm^{-1}, while the right panel is (b) $\lambda_3 = 0$ fm^{-1}.

APPENDIX: QMC OVERLAP WITH $G_\delta = 0$

The results (Sec. III) are replicated with no isovector scalar meson, i.e., $G_\delta = 0$ fm^2. As shown by Motta *et al.*, the isovector δ increases the maximum mass only marginally but changes the radius significantly [39]. For brevity, not all the results are included; only the preferred values of the overlap parameters are shown ($E_0 = 5500$ MeV and $b = 0.5$ fm). One finds that the largest effect of the change in G_δ is that the slope of the symmetry energy, L, decreases to 53 MeV for $\lambda_3 = 0.02$ fm^{-1} (52 MeV for $\lambda_3 = 0$ fm^{-1}).

The species fractions are given in Fig. 6. The Λ appears sooner without the δ meson, while the $\Xi^{0,-}$ both appear later.

Figure 7 shows the EoS, with the corresponding MR curve in Fig. 8. As expected, there is a slight decrease in the mass

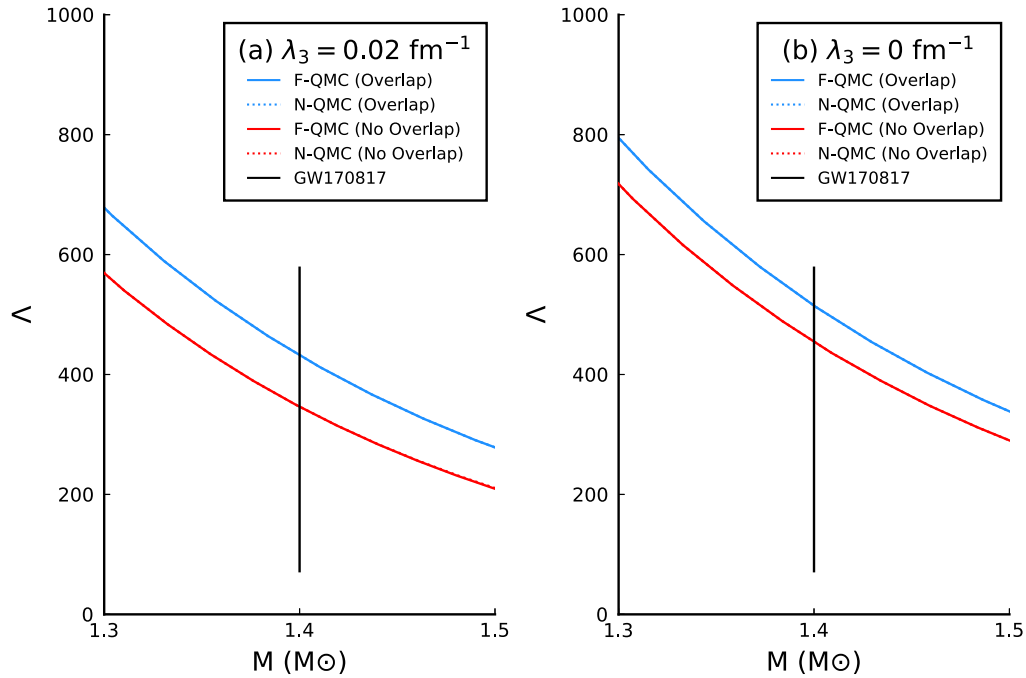

FIG. 9. Tidal deformation with $G_\delta = 0$ fm^2 with (a) $\lambda_3 = 0.02$ fm^{-1} and (b) $\lambda_3 = 0$ fm^{-1}.

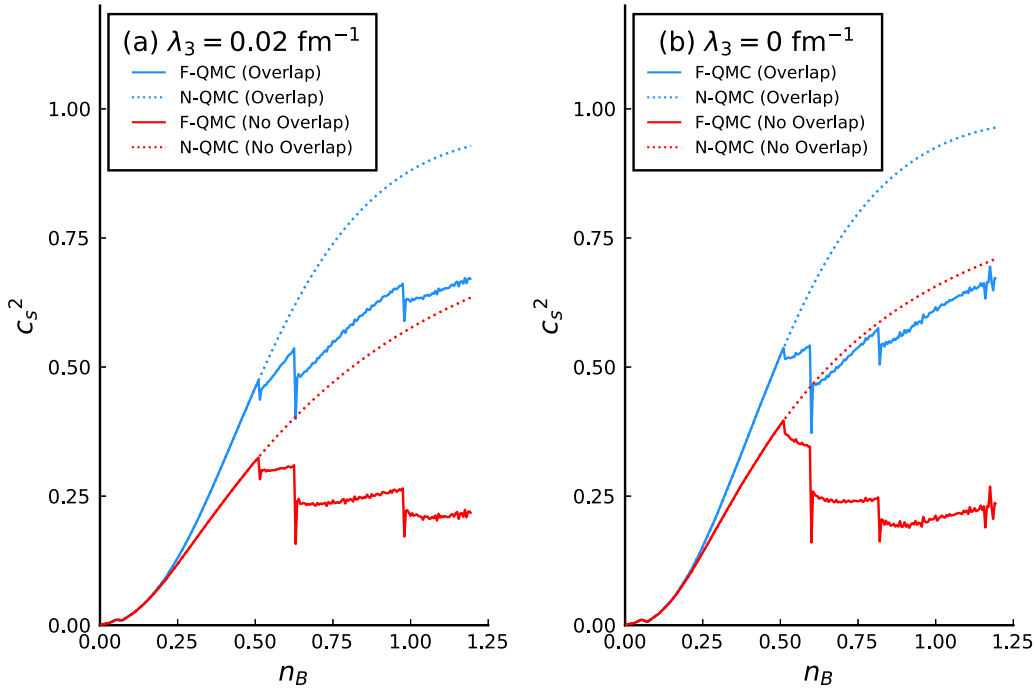

FIG. 10. Speed of sound (c_s^2) when $G_\delta = 0$ fm^2 with values of (a) $\lambda_3 = 0.02$ fm^{-1} and (b) $\lambda_3 = 0$ fm^{-1}.

and a substantial reduction in the radius. Without overlap and λ_3, the results show the same pattern reported in Ref. [39]. The reduction in the radius has an impact in the tidal deformability, which is presented in Fig. 9. In Fig. 4(b) we saw that the $\lambda_3 = 0$ fm^{-1} tidal deformation lay at the upper end of the experimental bound reported in Ref. [24]. However, with the reduction of the radii resulting when the δ meson is excluded, QMC with overlap now falls within GW170817 constraints. Again the inclusion of the σ^3 term with $\lambda_3 = 0.02$ fm^{-1} reduced the radius and fit the GW170817 constraint. Finally the speed of sound is shown in Fig. 10. The interpretation of these results may be found in Sec. III E.

[1] N. K. Glendenning, *Compact Stars: Nuclear Physics, Particle Physics and General Relativity*, Astronomy and Astrophysics Library (Springer, New York, 1997).

[2] S. L. Shapiro and S. A. Teukolsky, *Black Holes, White Dwarfs, and Neutron Stars: The Physics of Compact Objects* (Wiley, New York, 1983).

[3] J. R. Stone, Nuclear physics and astrophysics constraints on the high density matter equation of state, Universe **7**, 257 (2021).

[4] S. Gandolfi, A. Y. Illarionov, K. E. Schmidt, F. Pederiva, and S. Fantoni, Quantum Monte Carlo calculation of the equation of state of neutron matter, Phys. Rev. C **79**, 054005 (2009).

[5] T. Krüger, I. Tews, K. Hebeler, and A. Schwenk, Neutron matter from chiral effective field theory interactions, Phys. Rev. C **88**, 025802 (2013).

[6] E. Annala, T. Gorda, A. Kurkela, J. Nättilä, and A. Vuorinen, Evidence for quark-matter cores in massive neutron stars, Nat. Phys. **16**, 907 (2020).

[7] T. Kojo, P. D. Powell, Y. Song, and G. Baym, Phenomenological QCD equation of state for massive neutron stars, Phys. Rev. D **91**, 045003 (2015).

[8] T. Kojo, P. D. Powell, Y. Song, and G. Baym, Phenomenological QCD equations of state for neutron stars, Nucl. Phys. A **956**, 821 (2016).

[9] A. Kurkela, E. S. Fraga, J. Schaffner-Bielich, and A. Vuorinen, Constraining neutron star matter with quantum chromodynamics, Astrophys. J. **789**, 127 (2014).

[10] P. Danielewicz, R. Lacey, and W. G. Lynch, Determination of the equation of state of dense matter, Science **298**, 1592 (2002).

[11] J. R. Stone, P. Danielewicz, and Y. Iwata, Coulomb effects in low- and medium-energy heavy-ion collisions, Phys. Lett. B **826**, 136915 (2022).

[12] K. Masuda, T. Hatsuda, and T. Takatsuka, Hadron-quark crossover and massive hybrid stars with strangeness, Astrophys. J. **764**, 12 (2013).

[13] T. F. Motta and A. W. Thomas, The role of baryon structure in neutron stars, Mod. Phys. Lett. A **37**, 2230001 (2022).

[14] P. Freire, Pulsar mass measurements and tests of general relativity, https://www3.mpifr-bonn.mpg.de/staff/pfreire/NS_masses.html (2022).

[15] F. Özel and P. Freire, Masses, radii, and the equation of state of neutron stars, Annu. Rev. Astron. Astrophys. **54**, 401 (2016).

[16] A. W. Steiner, S. Gandolfi, F. J. Fattoyev, and W. G. Newton, Using neutron star observations to determine crust thicknesses, moments of inertia, and tidal deformabilities, Phys. Rev. C **91**, 015804 (2015).

[17] D. Chatterjee and I. Vidaña, Do hyperons exist in the interior of neutron stars?, Eur. Phys. J. A **52**, 29 (2016).

[18] G. F. Burgio, H. J. Schulze, I. Vidana, and J. B. Wei, Neutron stars and the nuclear equation of state, Prog. Part. Nucl. Phys. **120**, 103879 (2021).

[19] J. Antoniadis *et al.*, A massive pulsar in a compact relativistic binary, Science **340**, 1233232 (2013).

[20] Z. Arzoumanian *et al.* (NANOGrav Collaboration), The NANOGrav 11-year data set: High-precision timing of 45 millisecond pulsars, Astrophys. J. Suppl. Ser. **235**, 37 (2018).

[21] T. E. Riley *et al.*, A NICER view of the massive pulsar PSR J0740+6620 informed by radio timing and XMM-Newton spectroscopy, Astrophys. J. Lett. **918**, L27 (2021).

[22] E. Fonseca *et al.*, Refined mass and geometric measurements of the high-mass PSR J0740+6620, Astrophys. J. Lett. **915**, L12 (2021).

[23] M. Al-Mamun, A. W. Steiner, J. Nättilä, J. Lange, R. O'Shaughnessy, I. Tews, S. Gandolfi, C. Heinke, and S. Han, Combining Electromagnetic and Gravitational-Wave Constraints on Neutron-Star Masses and Radii, Phys. Rev. Lett. **126**, 061101 (2021).

[24] B. P. Abbott *et al.* (LIGO Scientific, Virgo Collaborations), GW170817: Measurements of Neutron Star Radii and Equation of State, Phys. Rev. Lett. **121**, 161101 (2018).

[25] B. P. Abbott *et al.* (LIGO Scientific, Virgo Collaborations), GW190425: Observation of a compact binary coalescence with total mass $\sim 3.4 M_{\odot}$, Astrophys. J. Lett. **892**, L3 (2020).

[26] K. Chatziioannou, K. Yagi, A. Klein, N. Cornish, and N. Yunes, Probing the internal composition of neutron stars with gravitational waves, Phys. Rev. D **92**, 104008 (2015).

[27] K. Chatziioannou, Neutron star tidal deformability and equation of state constraints, Gen. Relativ. Gravit. **52**, 109 (2020).

[28] P. Demorest, T. Pennucci, S. Ransom, M. Roberts, and J. Hessels, Shapiro delay measurement of a two solar mass neutron star, Nature (London) **467**, 1081 (2010).

[29] M. Baldo and G. F. Burgio, Properties of the nuclear medium, Rep. Prog. Phys. **75**, 026301 (2012).

[30] P. A. M. Guichon, A possible quark mechanism for the saturation of nuclear matter, Phys. Lett. B **200**, 235 (1988).

[31] P. A. M. Guichon, K. Saito, E. N. Rodionov, and A. W. Thomas, The Role of nucleon structure in finite nuclei, Nucl. Phys. A **601**, 349 (1996).

[32] P. A. M. Guichon, H. H. Matevosyan, N. Sandulescu, and A. W. Thomas, Physical origin of density dependent force of the Skyrme type within the quark meson coupling model, Nucl. Phys. A **772**, 1 (2006).

[33] P. A. M. Guichon and A. W. Thomas, Quark Structure and Nuclear Effective Forces, Phys. Rev. Lett. **93**, 132502 (2004).

[34] J. Rikovska Stone, P. A. M. Guichon, H. H. Matevosyan, and A. W. Thomas, Cold uniform matter and neutron stars in the quark-mesons-coupling model, Nucl. Phys. A **792**, 341 (2007).

[35] N. K. Glendenning, First order phase transitions with more than one conserved charge: Consequences for neutron stars, Phys. Rev. D **46**, 1274 (1992).

[36] D. L. Whittenbury, H. H. Matevosyan, and A. W. Thomas, Hybrid stars using the quark-meson coupling and proper-time Nambu–Jona-Lasinio models, Phys. Rev. C **93**, 035807 (2016).

[37] T. F. Motta, P. A. M. Guichon, and A. W. Thomas, On the sound speed in hyperonic stars, Nucl. Phys. A **1009**, 122157 (2021).

[38] J. R. Stone, V. Dexheimer, P. A. M. Guichon, A. W. Thomas, and S. Typel, Equation of state of hot dense hyperonic matter in the quark–meson-coupling (QMC-A) model, Mon. Not. Roy. Astron. Soc. **502**, 3476 (2021).

[39] T. F. Motta, A. M. Kalaitzis, S. Antić, P. A. M. Guichon, J. R. Stone, and A. W. Thomas, Isovector effects in neutron stars, radii and the GW170817 constraint, Astrophys. J. **878**, 159 (2019).

[40] P. A. M. Guichon, J. R. Stone, and A. W. Thomas, Quark–meson-coupling (QMC) model for finite nuclei, nuclear matter and beyond, Prog. Part. Nucl. Phys. **100**, 262 (2018).

[41] K. M. L. Martinez, A. W. Thomas, J. R. Stone, and P. A. M. Guichon, Parameter optimization for the latest quark-meson coupling energy-density functional, Phys. Rev. C **100**, 024333 (2019).

[42] K. M. L. Martinez, A. W. Thomas, P. A. M. Guichon, and J. R. Stone, Tensor and pairing interactions within the quark-meson coupling energy-density functional, Phys. Rev. C **102**, 034304 (2020).

[43] J. R. Stone, K. Morita, P. A. M. Guichon, and A. W. Thomas, Physics of even-even superheavy nuclei with $96 < Z < 110$ in the quark-meson-coupling model, Phys. Rev. C **100**, 044302 (2019).

[44] J. Stone, P. Guichon, and A. Thomas, Superheavy nuclei in the quark-meson-coupling model, EPJ Web Conf. **163**, 00057 (2017).

[45] J. R. Stone, P. A. M. Guichon, and A. W. Thomas, Nuclear symmetry energy and hyperonic stars in the QMC model, Front. Astron. Space Sci. **9**, 903007 (2022).

[46] A. Chodos, R. L. Jaffe, K. Johnson, and C. B. Thorn, Baryon structure in the bag theory, Phys. Rev. D **10**, 2599 (1974).

[47] A. W. Thomas, Chiral symmetry and the bag model: A new starting point for nuclear physics, Adv. Nucl. Phys. **13**, 1 (1984).

[48] F. Bissey, F.-G. Cao, A. R. Kitson, A. I. Signal, D. B. Leinweber, B. G. Lasscock, and A. G. Williams, Gluon flux-tube distribution and linear confinement in baryons, Phys. Rev. D **76**, 114512 (2007).

[49] J. M. Berryman and S. Gardner, Neutron star structure with a new force between quarks, Phys. Rev. C **104**, 045802 (2021).

[50] T. Inoue, N. Ishii, S. Aoki, T. Doi, T. Hatsuda, Y. Ikeda, K. Murano, H. Nemura, and K. Sasaki (HAL QCD Collaboration), Baryon-baryon interactions in the flavor SU(3) limit from full QCD simulations on the lattice, Prog. Theor. Phys. **124**, 591 (2010).

[51] J. M. Berryman, S. Gardner, and M. Zakeri, Neutron stars with baryon number violation, probing dark sectors, Symmetry **14**, 518 (2022).

[52] M. Harvey, Effective nuclear forces in the quark model with Delta and hidden color channel coupling, Nucl. Phys. A **352**, 326 (1981).

[53] T. Iritani, S. Aoki, T. Doi, S. Gongyo, T. Hatsuda, Y. Ikeda, T. Inoue, N. Ishii, H. Nemura, and K. Sasaki (HAL QCD Collaboration), Systematics of the HAL QCD potential at low energies in lattice QCD, Phys. Rev. D **99**, 014514 (2019).

[54] G. Q. Liu, M. Swift, A. W. Thomas, and K. Holinde, The role of nucleon structure in the NN interaction: Effects of pion exchange between quarks, Nucl. Phys. A **556**, 331 (1993).

[55] A. W. Thomas, Chiral symmetry and the bag model, Nucl. Phys. A **416**, 69 (1984).

[56] P. A. M. Guichon, A. W. Thomas, and K. Tsushima, Binding of hypernuclei in the latest quark-meson coupling model, Nucl. Phys. A **814**, 66 (2008).

[57] D. L. Whittenbury, J. D. Carroll, A. W. Thomas, K. Tsushima, and J. R. Stone, Quark-meson coupling model, nuclear matter

constraints and neutron star properties, Phys. Rev. C **89**, 065801 (2014).
[58] G. Krein, A. W. Thomas, and K. Tsushima, Fock terms in the quark meson coupling model, Nucl. Phys. A **650**, 313 (1999).
[59] J. Haidenbauer, K. Holinde, and A. W. Thomas, Investigation of pion exchange in the NN and $N\bar{N}$ systems, Phys. Rev. C **45**, 952 (1992).
[60] B.-A. Li and X. Han, Constraining the neutron-proton effective mass splitting using empirical constraints on the density dependence of nuclear symmetry energy around normal density, Phys. Lett. B **727**, 276 (2013).
[61] J. R. Stone, N. J. Stone, and S. A. Moszkowski, Incompressibility in finite nuclei and nuclear matter, Phys. Rev. C **89**, 044316 (2014).
[62] M. Dutra, O. Lourenco, J. S. Sa Martins, A. Delfino, J. R. Stone, and P. D. Stevenson, Skyrme interaction and nuclear matter constraints, Phys. Rev. C **85**, 035201 (2012).
[63] M. M. Sharma, The Breathing-mode giant monopole resonance and the surface compressibility in the relativistic mean-field theory, Nucl. Phys. A **816**, 65 (2009).
[64] J. Piekarewicz, Correlating the giant monopole resonance to the nuclear matter incompressibility, Phys. Rev. C **66**, 034305 (2002).
[65] R. Shyam and K. Tsushima, Description of the recently observed hypernucleus ${}^{15}_{\Xi^-}$C within a quark-meson coupling model, arXiv:1901.06090.
[66] C. J. Batty, E. Friedman, and A. Gal, Density dependence in Σ^- atoms and implications for Σ hypernuclei, Prog. Theor. Phys. Suppl. **117**, 227 (1994).
[67] T. F. Motta, A. W. Thomas, and P. A. M. Guichon, Do delta baryons play a role in neutron stars?, Phys. Lett. B **802**, 135266 (2020).
[68] O. Hashimoto and H. Tamura, Spectroscopy of Λ hypernuclei, Prog. Part. Nucl. Phys. **57**, 564 (2006).
[69] K. Nakazawa *et al.*, The first evidence of a deeply bound state of $\mathrm{Xi}^- - {}^{14}\mathrm{N}$ system, Prog. Theor. Exp. Phys. **2015**, 033D02 (2015).
[70] N. Chamel, A. F. Fantina, J. L. Zdunik, and P. Haensel, Neutron drip transition in accreting and nonaccreting neutron star crusts, Phys. Rev. C **91**, 055803 (2015).
[71] D. G. Yakovlev, A. D. Kaminker, O. Y. Gnedin, and P. Haensel, Neutrino emission from neutron stars, Phys. Rep. **354**, 1 (2001).
[72] S. Antić, J. R. Stone, J. C. Miller, K. L. Martinez, P. A. M. Guichon, and A. W. Thomas, Outer crust of a cold, nonaccreting neutron star within the quark-meson-coupling model, Phys. Rev. C **102**, 065801 (2020).
[73] M. Hempel and J. Schaffner-Bielich, Statistical model for a complete supernova equation of state, Nucl. Phys. A **837**, 210 (2010).
[74] M. Hempel, T. Fischer, J. Schaffner-Bielich, and M. Liebendorfer, New equations of state in simulations of core-collapse supernovae, Astrophys. J. **748**, 70 (2012).
[75] L. Meng and D.-J. Liu, Tidal Love numbers of neutron stars in Rastall gravity, Astrophys. Space Sci. **366**, 105 (2021).
[76] Y.-M. Kim, Y. Lim, K. Kwak, C. H. Hyun, and C.-H. Lee, Tidal deformability of neutron stars with realistic nuclear energy density functionals, Phys. Rev. C **98**, 065805 (2018).